


## Article

# Chemical Constituents of the Deep-Sea-Derived *Penicillium citreonigrum* MCCC 3A00169 and Their Antiproliferative Effects

Zheng-Biao Zou <sup>1,2,†</sup>, Gang Zhang <sup>3,†</sup>, Yu-Qi Zhou <sup>4,†</sup>, Chun-Lan Xie <sup>2</sup>, Ming-Min Xie <sup>2</sup>, Lin Xu <sup>2</sup>, You-Jia Hao <sup>2</sup>, Lian-Zhong Luo <sup>3</sup>, Xiao-Kun Zhang <sup>4,\*</sup>, Xian-Wen Yang <sup>2,\*</sup>  and Jun-Song Wang <sup>1,\*</sup>

<sup>1</sup> Center for Molecular Metabolism, School of Environmental and Biological Engineering, Nanjing University of Science and Technology, 200 Xiaolingwei Street, Nanjing 210094, China

<sup>2</sup> Key Laboratory of Marine Genetic Resources, Third Institute of Oceanography, Ministry of Natural Resources, 184 Daxue Road, Xiamen 361005, China

<sup>3</sup> Xiamen Key Laboratory of Marine Medicinal Natural Products Resources, Xiamen Medica College, 1999 Guankouzhong Road, Xiamen 361023, China

<sup>4</sup> School of Pharmaceutical Sciences, Xiamen University, South Xiang'an Road, Xiamen 361102, China

\* Correspondence: xkzhang@xmu.edu.cn (X.-K.Z.); yangxianwen@tio.org.cn (X.-W.Y.); wangjunsong@njjust.edu.cn (J.-S.W.); Tel.: +86-592-2181851 (X.-K.Z.); +86-592-2195319 (X.-W.Y.); +86-258-4315512 (J.-S.W.)

† These authors contributed equally to this work.

**Abstract:** Six new citreoviridins (citreoviridins J–O, 1–6) and twenty-two known compounds (7–28) were isolated from the deep-sea-derived *Penicillium citreonigrum* MCCC 3A00169. The structures of the new compounds were determined by spectroscopic methods, including the HRESIMS, NMR, ECD calculations, and dimolybdenum tetraacetate-induced CD (ICD) experiments. Citreoviridins J–O (1–6) are diastereomers of 6,7-epoxycitreoviridin with different chiral centers at C-2–C-7. Pyrenocine A (7), terrein (14), and citreoviridin (20) significantly induced apoptosis for HeLa cells with IC<sub>50</sub> values of 5.4 μM, 11.3 μM, and 0.7 μM, respectively. To be specific, pyrenocine A could induce S phase arrest, while terrein and citreoviridin could obviously induce G0–G1 phase arrest. Citreoviridin could inhibit mTOR activity in HeLa cells.

**Keywords:** deep-sea; fungus; *Penicillium solitum*; anti-tumor; apoptosis



**Citation:** Zou, Z.-B.; Zhang, G.; Zhou, Y.-Q.; Xie, C.-L.; Xie, M.-M.; Xu, L.; Hao, Y.-J.; Luo, L.-Z.; Zhang, X.-K.; Yang, X.-W.; et al. Chemical Constituents of the Deep-Sea-Derived *Penicillium citreonigrum* MCCC 3A00169 and Their Antiproliferative Effects. *Mar. Drugs* **2022**, *20*, 736. <https://doi.org/10.3390/md20120736>

Academic Editor: Bill J. Baker

Received: 21 October 2022

Accepted: 20 November 2022

Published: 24 November 2022

**Publisher's Note:** MDPI stays neutral with regard to jurisdictional claims in published maps and institutional affiliations.



**Copyright:** © 2022 by the authors. Licensee MDPI, Basel, Switzerland. This article is an open access article distributed under the terms and conditions of the Creative Commons Attribution (CC BY) license (<https://creativecommons.org/licenses/by/4.0/>).

## 1. Introduction

*Penicillium citreonigrum* is a commonly found fungus known for its contamination of rice with citreoviridin (CTV), a yellow mycotoxin related to the disease of acute cardiac beriberi [1]. In addition to CTV, *P. citreonigrum* can also produce other structurally diverse compounds, including azaphilones [2], chromones [3], alkaloids [3–5], sesquiterpenes [6,7], meroterpenes [2], etc. Most of these compounds showed cytotoxicity against different tumor cells. For example, 2-hydroxyl-3-pyrenocine-thio propanoic acid, a sulfur-containing polyketone isolated from a deep-sea-derived *P. citreonigrum* XT20-134, showed a potent effect against Bel-7402 tumor cells with an IC<sub>50</sub> value of 7.6 μM [5]; sclerotioramine, a chlorinated alkaloid obtained from the terrestrial *P. citreonigrum*, exhibited moderate activity against the HepG2 cell line with an IC<sub>50</sub> value of 7.3 μg/mL [3].

Due to their ability to produce new secondary metabolites, deep-sea-derived microorganisms have attracted more and more attention [8]. As part of our continuous investigations on deep-sea-derived fungi [9–11], *P. citreonigrum* MCCC 3A00169 was subjected for a systematic chemical study. Consequently, 6 new CTVs (citreoviridins J–O, 1–6, Figure 1) and 22 known compounds (7–28, Figure S1) were obtained. We report herein the fermentation, isolation, structure, and bioactivities of these secondary metabolites.

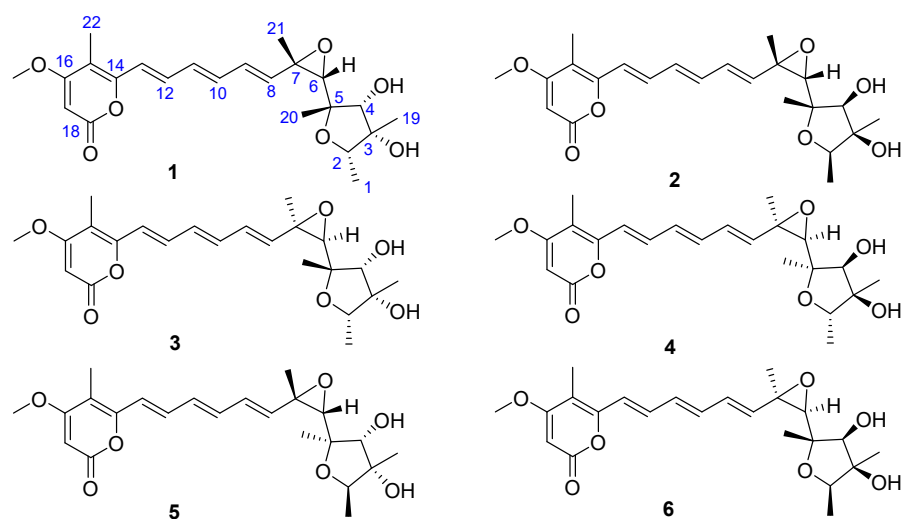


Figure 1. Compounds 1–6 from the deep-sea-derived *Penicillium citreonigrum* MCCC 3A0016.

## 2. Results and Discussion

The EtOAc extract of the fermentation broth of *P. citreonigrum* MCCC 3A00169 was subjected to extensive column chromatography (CC) over silica gel, ODS, and Sephadex LH-20. Final purification by semi-preparative HPLC yielded compounds 1–28. By a comparison of the NMR and MS data with references, 22 previously reported components were identified as pyrenocine A (7) [12], cerebrosides A (8) [13], ergosterol (9) [14],  $\beta$ -sitosterol (10) [15], dehydrololiolide (11) [16], 3-hydroxy-4-methoxycinnamic acid (12) [17], terrein-d-glucoside (13) [18], terrein (14) [18], microsphaerone B (15) [19], surfactin C15 (16) [20], butyrolactone V (17) [21], microsphaerone A (18) [19], butyrolactone I (19) [22], citreoviridin (20) [23], isocitreoviridin (21) [24], (+)-cyclophenol (22) [25], tryptamine (23) [26], 1*H*-indole-3-carboxylic acid (24) [27], pyrenocine B (25) [28], citreo- $\gamma$ -pyrone (26) [29], de-*O*-methyladiaporthin (27) [30], and 3,4-dihydro-3,4,8-trihydroxy-1(2*H*)-naphthalenon (28) [31].

Compound 1 was assigned a molecular formula  $C_{23}H_{30}O_7$  according to the protonated ion peak at  $m/z$  419.2049 (calcd for  $C_{23}H_{31}O_7$ , 419.2064) in its HR-ESI-MS spectrum (Figure S2), requiring nine double-bond equivalents. The  $^1H$  and  $^{13}C$  NMR spectroscopic data (Tables 1 and 2, Figures S3 and S4) showed one methyl doublet and four methyl singlets, one methoxyl, ten methines (three oxygenated and seven olefinic carbons), and six quaternary carbons (three olefinic carbons and one carbonyl carbon). A close comparison of the NMR data for 1 with those of the citreoviridin I, a CTV isolated from a mangrove endophytic fungus *Penicillium* sp. BJR-P2 [32], indicated that they were structurally similar. Further analysis of their HR-ESI-MS data revealed that 1 was the dehydration product of citreoviridin I. The speculation was clearly evidenced by the HMBC correlations (Figure 2) from H<sub>3</sub>-21 ( $\delta_H$  1.35, s) to C-6 ( $\delta_C$  84.3)/C-7 ( $\delta_C$  77.2)/C-8 ( $\delta_C$  144.7), H-8 ( $\delta_H$  6.41, d,  $J$  = 15.2 Hz) to C-7 ( $\delta_C$  77.2), H-6 ( $\delta_H$  3.60, s) to C-8 ( $\delta_C$  144.7), and H<sub>3</sub>-20 ( $\delta_H$  1.23, s) to C-6 ( $\delta_C$  84.3).

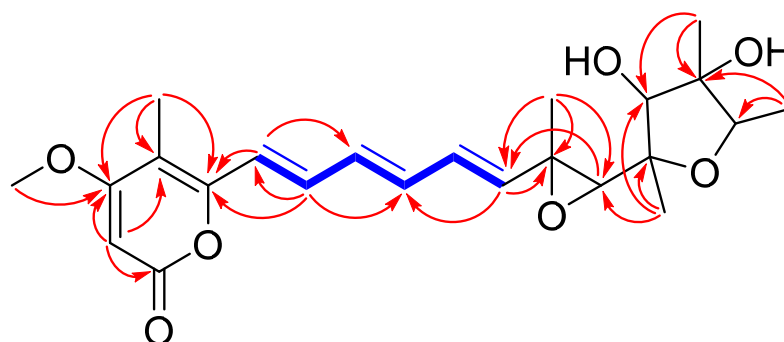
The relative configuration of 1 was determined by coupling constants analysis and an NOESY experiment. *E*-configurations for three double bonds of  $\Delta^{8,10,12}$  were identified on the basis of the large coupling constants of  $^3J_{8,9}$  (15.2 Hz),  $^3J_{10,11}$  (14.8 Hz), and  $^3J_{12,13}$  (15.2 Hz), respectively (Table 1). A *cis* relationship between H<sub>3</sub>-21 and H-6 was established for their distinct NOESY cross-peak (Figure 3). The relative configuration of the 2,3,5-trimethyl-tetrahydro-furan-3,4-diol in 1 was elucidated as 2*S*\*,3*S*\*,4*R*\*,5*S*\* according to the NOESY correlations of H-2 ( $\delta_H$  3.92, q,  $J$  = 6.4 Hz) with H<sub>3</sub>-19 ( $\delta_H$  1.29, s) and of H-4 with H<sub>3</sub>-19 and H-6.

**Table 1.** The  $^1\text{H}$  (400 MHz) NMR data of compounds 1–6 in  $\text{CD}_3\text{OD}$  ( $J$  in Hz).

No.	1	2	3	4	5	6
1	1.15 d (6.4)	1.17 d (6.4)	1.33 d (6.4)	1.19 d (6.4) <sup>a</sup>	1.20 d (6.4)	1.19 d (6.4)
2	3.92 q (6.4) <sup>a</sup>	4.05 q (6.4)	4.27 q (6.4) <sup>a</sup>	4.10 q (6.4)	4.09 q (6.4) <sup>a</sup>	4.04 q (6.4) <sup>a</sup>
4	4.06 s	3.98 s	3.76 s	3.63 s	4.02 s	3.78 s
6	3.60 s	3.61 s	3.81 s	3.50 s	3.63 s	3.67 s
8	6.41 d (15.2)	6.06 d (15.2)	5.96 d (15.2)	6.56 d (15.2)	6.01 d (15.2)	6.02 d (15.2)
9	6.51 dd (14.8, 10.8)	6.42 dd (14.8, 10.8) <sup>a</sup>	6.57 <sup>a</sup>	6.38 dd (15.2, 10.8)	6.42 dd (15.2, 10.8) <sup>a</sup>	6.41 dd (15.2, 10.8) <sup>a</sup>
10	6.54 dd (14.8, 10.8)	6.51 dd (14.8, 10.8) <sup>a</sup>	6.58 <sup>a</sup>	6.61 dd (14.8, 10.8) <sup>a</sup>	6.60 dd (14.8, 10.8) <sup>a</sup>	6.64 dd (15.2, 10.8) <sup>a</sup>
11	6.47 dd (14.8, 10.8) <sup>a</sup>	6.48 dd (15.2, 10.8)	6.48 <sup>a</sup>	6.46 dd (14.8, 10.8) <sup>a</sup>	6.48 dd (14.8, 10.8) <sup>a</sup>	6.50 dd (14.8, 11.2) <sup>a</sup>
12	7.14 dd (14.8, 10.8)	7.13 dd (15.2, 10.8)	7.12 dd (14.8, 10.8)	7.14 dd (14.8, 10.8)	7.14 dd (14.8, 10.8)	7.16 dd (15.2, 10.8)
13	6.49 d (15.2)	6.55 d (15.2)	6.60 d (14.8) <sup>a</sup>	6.57 d (15.2) <sup>a</sup>	6.59 d (15.2) <sup>a</sup>	6.60 d (15.2) <sup>a</sup>
17	5.62 s	5.62 s	5.62 s	5.62 s	5.63 s	5.63 s
19	1.29 s	1.28 s	1.21 s	1.17 s	1.18 s	1.28 s
20	1.23 s	1.25 s	1.21 s	1.30 s	1.27 s	1.20 s
21	1.35 s	1.30 s	1.30 s	1.45 s	1.29 s	1.31 s
22	2.00 s	2.00 s	2.00 s	2.00 s	2.01 s	2.01 s
OMe	3.90 s	3.90 s	3.91 s	3.91 s	3.90 s	3.91 s

<sup>a</sup> overlapped  $^1\text{H}$  NMR signals.**Table 2.**  $^{13}\text{C}$  (100 MHz) NMR data of compounds 1–6 in  $\text{CD}_3\text{OD}$ .

No.	1	2	3	4	5	6
1	13.6 q	13.5 q	12.1 q	13.5 q	13.8 q	13.8 q
2	79.2 d	80.9 d	81.9 d	80.2 d	80.0 d	79.8 d
3	84.1 s	84.5 s	85.2 s	86.0 s	84.9 s	84.3 s
4	74.8 d	80.9 d	81.7 d	79.3 d	79.4 d	79.1 d
5	84.3 s	84.8 s	87.4 s	85.1 s	87.5 s	87.3 s
6	84.1 d	76.5 d	85.5 d	82.2 d	91.0 d	92.0 d
7	77.2 s	79.8 s	76.9 s	79.7 s	74.3 s	74.3 s
8	144.7 d	148.5 d	144.0 d	143.6 d	143.5 d	141.9 d
9	129.0 d	128.7 d	129.4 d	129.1 d	129.5 d	129.4 d
10	139.7 d	138.9 d	138.8 d	140.0 d	139.1 d	139.1 d
11	131.7 d	132.5 d	132.6 d	132.0 d	132.5 d	132.4 d
12	137.3 d	137.0 d	137.1 d	137.3 d	137.1 d	137.1 d
13	120.0 d	120.4 d	120.4 d	120.0 d	120.4 d	120.3 d
14	156.0 s	155.9 s	155.9 s	156.0 s	155.9 s	155.9 s
15	109.6 s	109.8 s	109.8 s	109.6 s	109.8 s	109.8 s
16	173.2 s	173.1 s	173.1 s	173.1 s	173.1 s	173.1 s
17	89.0 d	89.1 d	89.1 d	89.0 d	89.1 d	89.1 d
18	166.4 s	166.4 s	166.4 s	166.4 s	166.4 s	166.4 s
19	17.5 q	17.5 q	13.1 q	17.3 q	13.2 q	13.1 q
20	16.6 q	18.7 q	14.4 q	16.7 q	14.6 q	14.6 q
21	32.2 q	26.7 q	26.6 q	31.2 q	26.2 q	27.3 q
22	8.9 q	8.9 q	8.9 q	8.9 q	8.9 q	8.9 q
OMe	57.3 q	57.3 q	57.3 q	57.3 q	57.3 q	57.3 q

**Figure 2.** The key COSY (bold) and HMBC (arrows) correlations of 1.

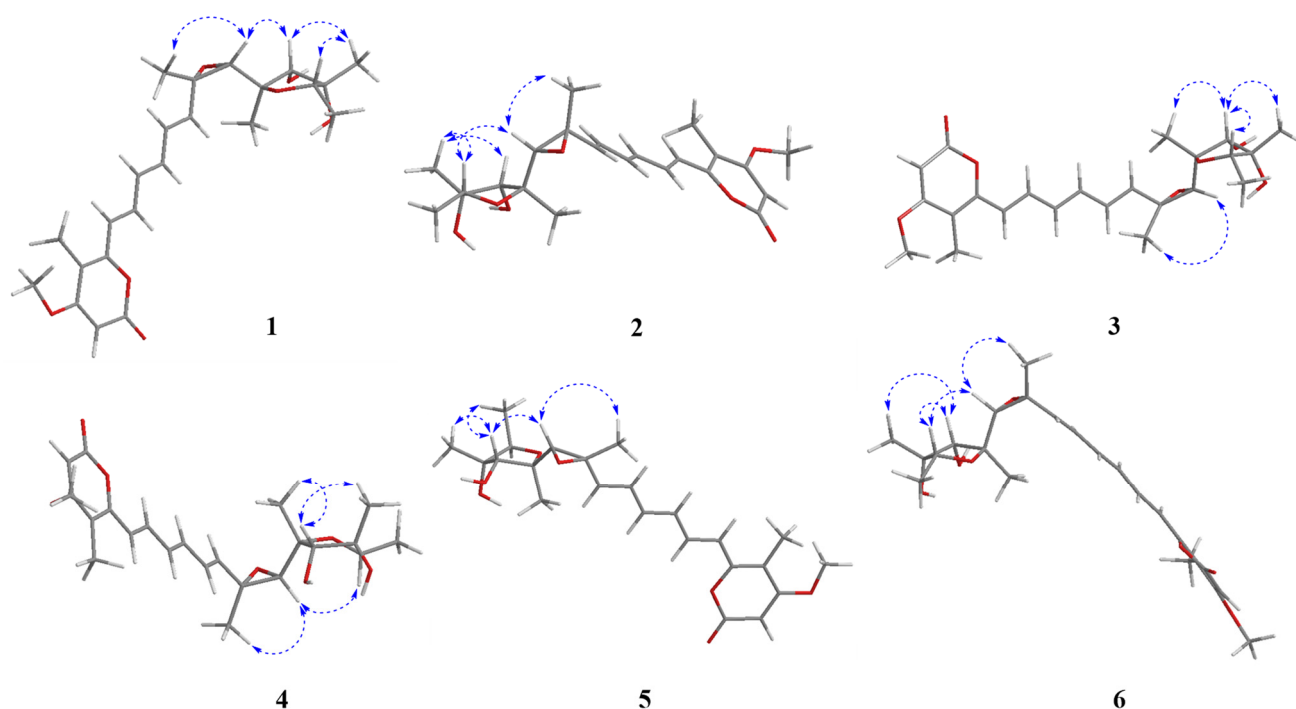


**Figure 3.** The key NOESY correlations of compounds 1–6.

To determine the absolute configurations at C-6 and C-7 in **1**, ECD calculations of the optimized conformations of (6*R*,7*R*)-**1** (**1a**) and (6*S*,7*S*)-**1** (**1b**) were obtained at the B3LYP/6-31+G(d) level. The agreement between the calculated ECD spectrum of **1b** and the experimental ECD spectrum (Figure 4A) suggested a 6*S*,7*S*-configuration for compound **1**.

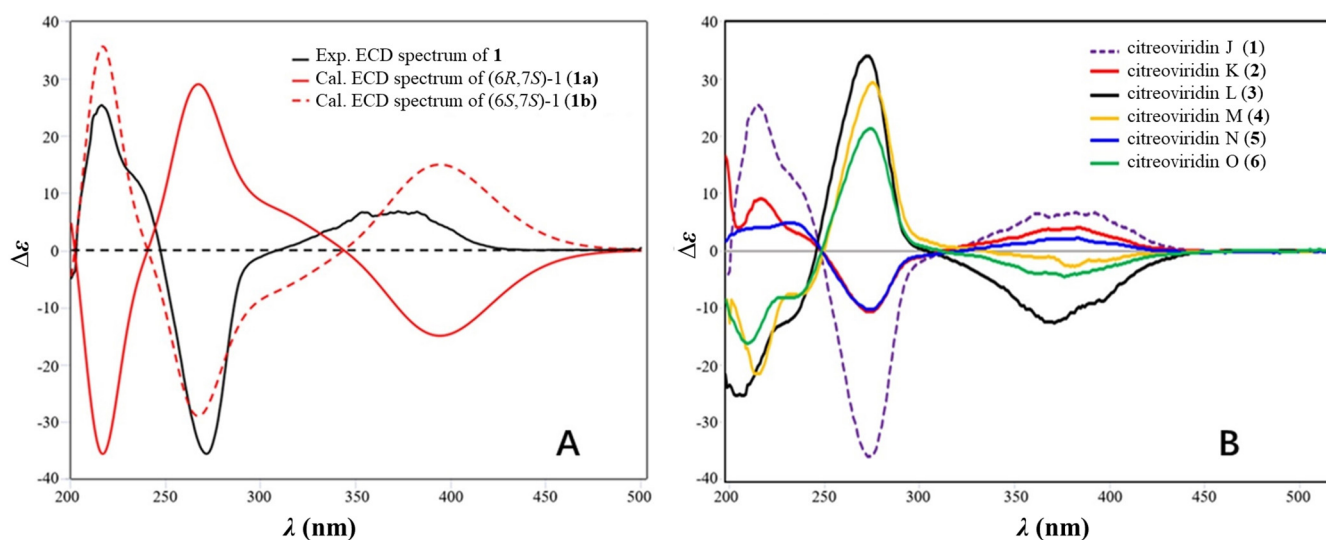


**Figure 4.** Calculated and experimental ECD spectra of **1** (A) and the experimental ECD spectra of **1–6** (B).

The absolute configuration of 2,3,5-trimethyl-tetrahydro-furan-3,4-diol residues was determined by a dimolybdenum tetraacetate [ $\text{Mo}_2(\text{OAc})_4$ ]-induced CD (ICD) experiment. Generally, 1, 2-diol compounds can react with  $\text{Mo}_2(\text{OAc})_4$  to form chiral complexes showing multiple Cotton effects in the range of 250–650 nm, of which the band near 310 nm is closely related to the absolute configuration of 1, 2-diol [33,34]. This method is also suitable for rigid cyclic 1, 2-diols [35,36]. In our experiments, the ICD spectrum of **1** exhibited a positive Cotton effect at 310 nm (Figure 5), suggesting a positive torsional angle for

the O–C–C–O moiety. It was ascertained that the 3*S*,4*R*-form could maintain the favored conformation (Scheme 1). Therefore, the absolute configuration of **1** was determined as (2*S*,3*S*,4*R*,5*S*,6*S*,7*S*)-6,7-dihydro-6,7-epoxycitreoviridin and named citreoviridin J.

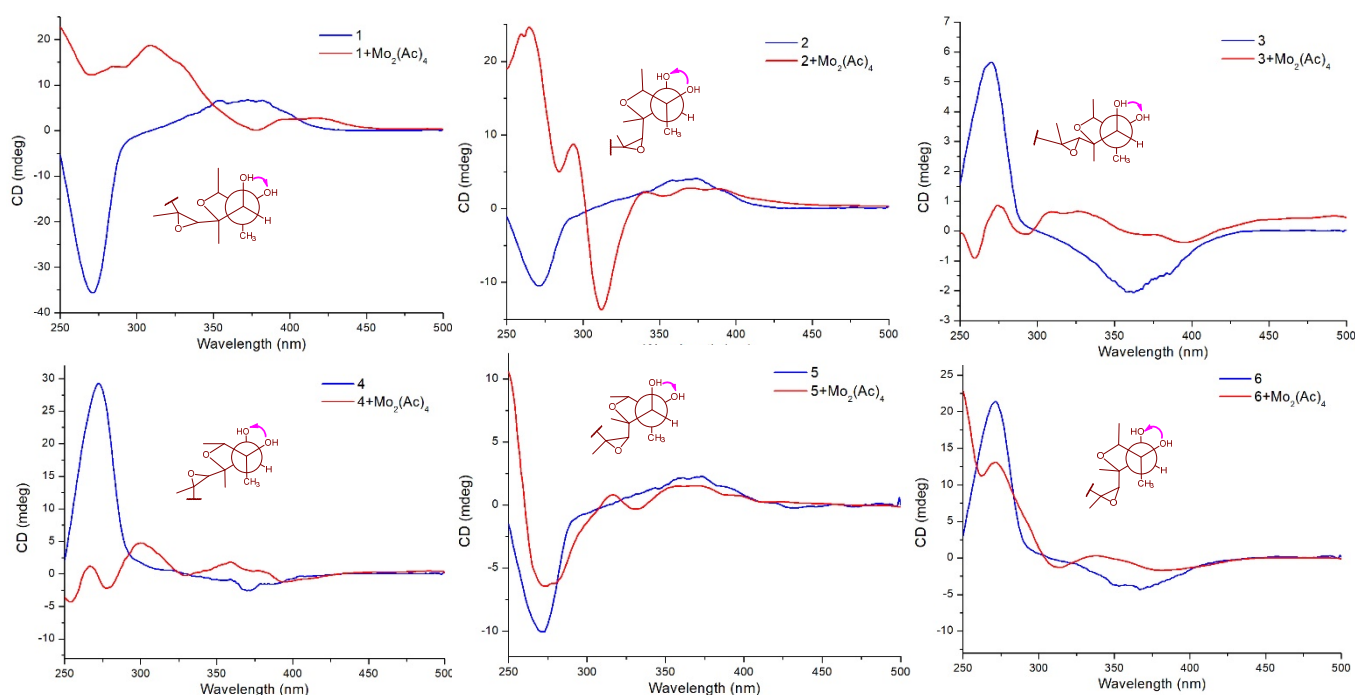
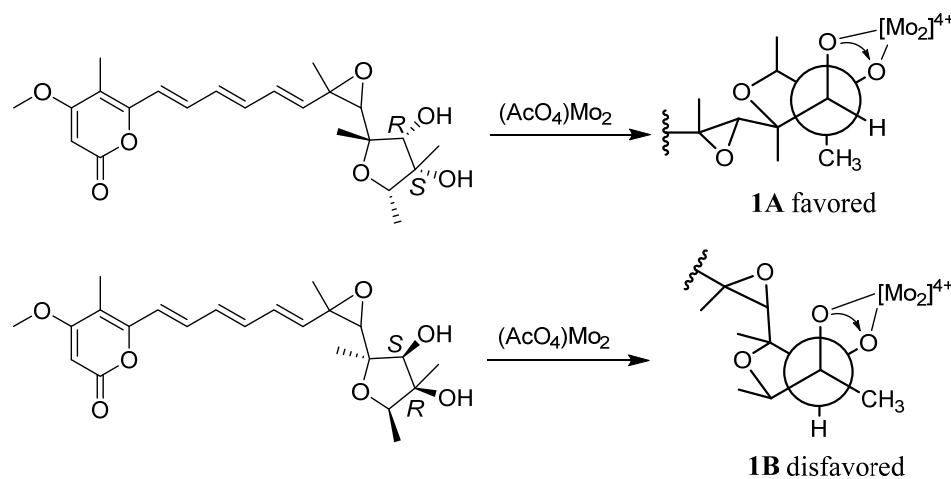


**Figure 5.** CD spectra and dimolybdenum tetraacetate [Mo<sub>2</sub>(OAc)<sub>4</sub>]-induced CD spectra of compounds 1–6.



**Scheme 1.** Conformers **1A** and **1B** of compound **1**.

An analysis of the <sup>1</sup>H and <sup>13</sup>C NMR spectroscopic data (Tables 1 and 2) and HR-ESI-MS data of compounds 2–6 revealed that they share the same planar structure of **1**. However, minor differences in the <sup>13</sup>C NMR chemical shift ranging from C-1 to C-7 indicated that 2–6 were diastereomers of **1** with different configurations in the 2,3,5-trimethyl-6-oxiranyl-tetrahydro-furan-3,4-diol residues.

Therefore, similar to **1**, NOESY, ECD, and ICD experiments and coupling constants analysis were also employed to determine the absolute configurations of 2–6. The geometry at Δ<sup>8,10,12</sup> double bonds in 2–6 was assigned as *E* based on the large coupling constants (*ca* 15 Hz). Likewise, the trans-configuration of epoxides and the cis-configuration for H-6 and H<sub>3</sub>-21 in 2–6 were assigned on the basis of the NOESY correlations of H-6 to H<sub>3</sub>-21 (Figure 3). The relative configurations of the 2,3,5-trimethyl-tetrahydro-furan-3,4-

diol residues in **2–6** were also elucidated based on NOESY correlations, as shown in Figure 3. The ECD spectra of **2** and **5** showed positive Cotton effects at 215 nm and 373 nm and negative Cotton effects at 270 nm (Figure 4), which were in accordance with that of **1**. Therefore, 6*S*,7*S*-configuration was assigned for **2** and **5**. On the contrary, 6*R*,7*R*-configuration was assigned for **3**, **4**, and **6** because of the mirror-like ECD spectra (Figure 4). Similar to that of **1**, the Mo<sub>2</sub>(OAc)<sub>4</sub>-induced CD spectra of **3** and **5** exhibited positive Cotton effects at 300–350 nm, indicating positive torsional angles for the O–C–C–O moieties (Figure 5). So, 3*S*,4*R*-configuration was defined for **3** and **5**. The negative Cotton effects at 300–350 nm represented negative torsional angles for the O–C–C–O moieties, establishing 3*R* and 4*S* configurations of **2**, **4**, and **6** (Figure 5). On the basis of the above evidence, the absolute configurations of **2–6** were defined as (2*R*,3*R*,4*S*,5*S*,6*S*,7*S*), (2*S*,3*S*,4*R*,5*S*,6*R*,7*R*), (2*S*,3*R*,4*S*,5*R*,6*R*,7*R*), (2*R*,3*S*,4*R*,5*R*,6*S*,7*S*), and (2*R*,3*R*,4*S*,5*S*,6*R*,7*R*), respectively, and were named as citreoviridins K–O.

All isolates were tested for antiproliferative activity against HeLa tumor cells. Compounds **7**, **14**, and **20** exhibited significant effects, with IC<sub>50</sub> values of 5.4 μM, 11.3 μM, and 0.7 μM, respectively (Figure 6A). To further detect the apoptosis activity of these three compounds, HeLa cells were analyzed by western blotting after treatment with **7**, **14**, and **20** for 40 h. The cleavage of PARP protein, a sensitive apoptotic marker, was used to detect the apoptosis activity. As shown in Figure 6B, they all induced potent apoptosis. It was reported that **20** could inhibit human umbilical vein endothelial cells (HUVECs) proliferation [37]. Compound **7** showed cytotoxicity against several cancer cells, with IC<sub>50</sub> values ranging from 2.6 to 12.9 μM. Terrein (**14**) displayed strong cytotoxicities against human breast cancer MCF-7 cells [38] and human lung cancer A<sub>549</sub> cells [39]. Hence, our findings were consistent with those reported in previous experiments, though different cancer cell lines were evaluated.

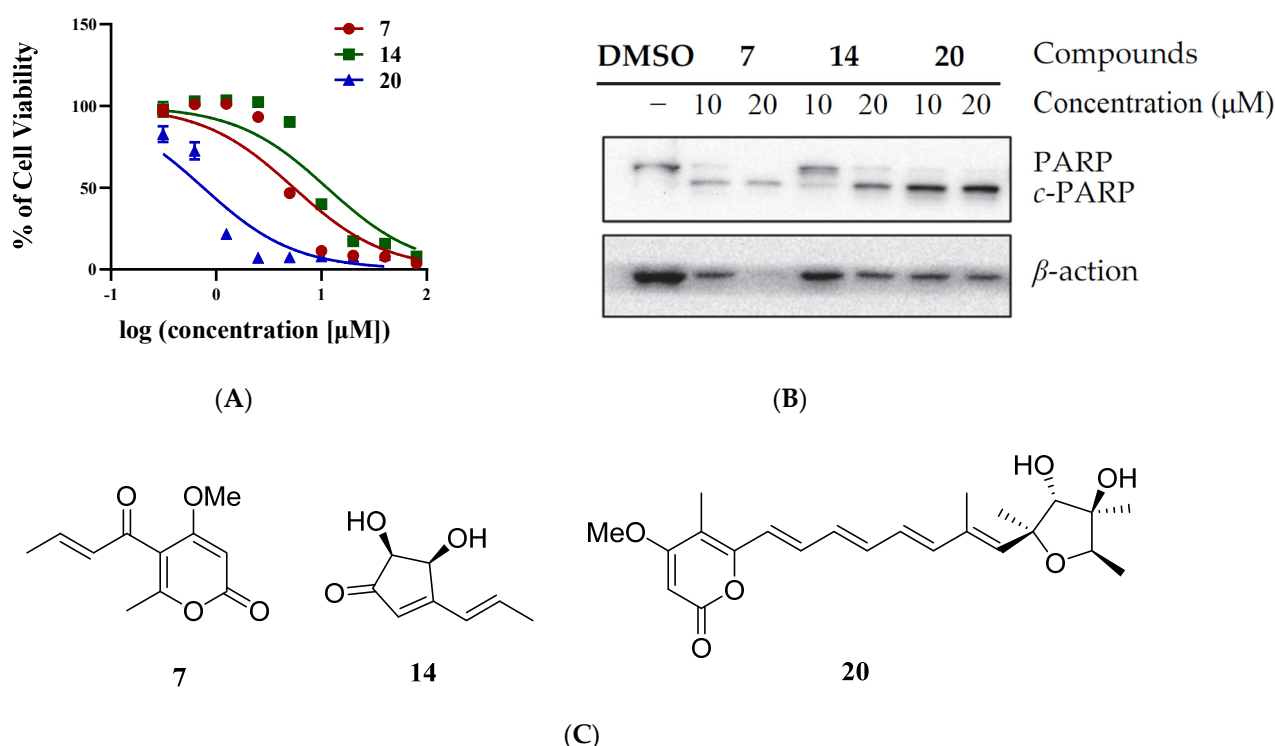


**Figure 6.** Antiproliferative effects of compounds **7**, **14**, and **20** on HeLa tumor cells. **(A)** The IC<sub>50</sub> values of tested compounds. **(B)** Apoptosis activity (HeLa cells were harvested after treatment with the tested compounds for 40 h; the related protein levels were analyzed by Western blot; the cleaved PARP bands indicate the apoptosis bioactivity). **(C)** Structures of compounds **7**, **14**, and **20**.

To detect their effect on cell cycle progression, HeLa cells were treated with compounds **7**, **14**, and **20** for 16 h, stained with propidium iodide, and analyzed by flow cytometry. As shown in Figure 7, **7** could induce S phase arrest, while **14** and **20** could obviously induce G0-G1 phase arrest. Compound **20** also inhibited the proliferation of HUVECs that were arrested at the G0/G1 phase [37].

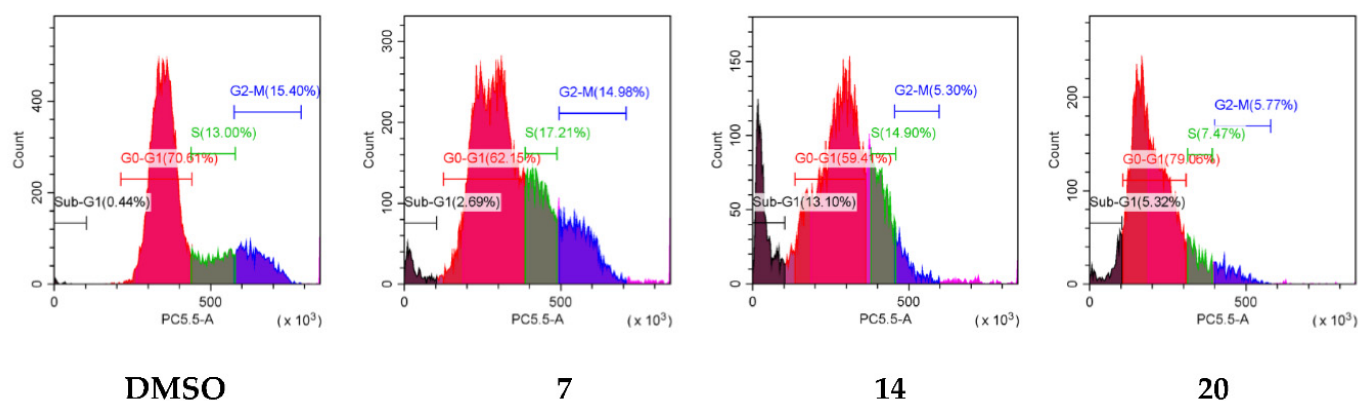


**Figure 7.** Effect of **7**, **14**, and **20** on cell cycle progression. HELA cells were stained by propidium iodide after treatment with **7** (20  $\mu$ M), **14** (20  $\mu$ M), and **20** (10  $\mu$ M) for 16 h.

As is known to all, the mTOR is one of the most usually activated signaling pathways in cancer. The major downstream target of the mTOR is the ribosomal protein S6.

Previously, citreoviridin induces myocardial apoptosis through the PPAR- $\gamma$ -mTORC2-mediated autophagic pathway [40]. Therefore, compound **20** detected the protein level of the phosphorylation of S6. As is shown in Figure 8, compound **20** was found to obviously inhibit p-S6, indicating that **20** could strongly inhibit the mTOR pathway. Therefore, compound **20** might induce apoptosis through mTOR inhibition.

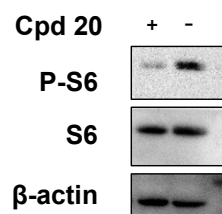


**Figure 8.** mTOR Inhibition induced by **20**. HeLa cells were treated with **20** (20  $\mu$ M) for 12 h. The protein level of the phosphorylation of ribosomal protein S6 was used to detect the mTOR activity.

### 3. Materials and Methods

#### 3.1. General Experimental Procedures

Optical rotations were recorded on an Anton Paar MCP 100 polarimeter. ECD spectra were recorded on a Chirascan spectropolarimeter. The HRESIMS spectra were recorded on Q-Exacte Focus tandem mass spectrometry. The NMR spectra were recorded on a Bruker AVANCE III 400 MHz spectrometer. The preparative and semipreparative HPLC were performed on an Agilent Technologies 1260 infinity instrument using ODS or Chiralpak IC columns. UV spectra were recorded on a UV-8000 UV/Vis spectrometer. Column chromatography (CC) was performed on silica gel and Sephadex LH-20. The TLC plates were visualized under UV light or by spraying with 10% H<sub>2</sub>SO<sub>4</sub>.

#### 3.2. Biological Material

The fungal strain *Penicillium citreonigrum* was isolated from the deep-sea sediment of the Northeastern Pacific at a depth of  $-2530$  m. The voucher strain was preserved at the Marine Culture Collection of China (MCCC, Xiamen, China) and was given the accession number MCCC 3A00169.

### 3.3. Fermentation and Extraction

*P. citreonigrum* MCCC 3A00169 was grown under static conditions at 25 °C in 85 × 1 L Erlenmeyer flasks, each containing 80 g of rice and 120 mL of distilled H<sub>2</sub>O. After 47 days, the fermentation broth was extracted by EtOAc three times to give a crude extract (32 g).

### 3.4. Isolation and Purification

The EtOAc-soluble extract was subjected to CC over silica gel using gradient CH<sub>2</sub>Cl<sub>2</sub>-MeOH to give six fractions (Fr.1–Fr.6). Fraction Fr.1 (7 g) was separated into three sub-fractions (Fr.1-1–Fr.1-3) by CC over ODS with MeOH-H<sub>2</sub>O (40%→100%). Fr.1-1 (31 mg) was further separated by HPLC (10%→40%→100%, MeOH-H<sub>2</sub>O) to yield **7** (22 mg, *t<sub>R</sub>* 32 min) and **11** (2 mg, *t<sub>R</sub>* 29 min). Fr.1-3 (0.7 g) was purified by CC over Sephadex LH-20 (MeOH) to yield **9** (5 mg) and **10** (54 mg). Fraction Fr.2 (0.9 g) was separated by Sephadex LH-20 (MeOH) to yield **12** (2 mg). Fraction Fr.3 (10.3 g) was purified by CC over ODS with MeOH-H<sub>2</sub>O (30%→100%) to yield eleven subfractions (Fr.3-1–Fr.3-11). Fr.3-1–Fr.3-6 was directly separated by Sephadex LH-20 (MeOH) to yield **14** (295 mg), **22** (10 mg), **23** (2 mg), **24** (2 mg), and **16** (694 mg), respectively. Fr.3-7 was further purified to CC over Sephadex LH-20 (MeOH) and HPLC (55%→80%, MeOH-H<sub>2</sub>O) to yield **17** (5 mg) and a mixture of **5** and **6**, which was further isolated by the IC chiral column using n-hexane isopropyl alcohol (55%) as the mobile phase to yield **5** (2 mg, *t<sub>R</sub>* 25.6 min) and **6** (2 mg, *t<sub>R</sub>* 26.5 min). Fr.3-8 (877 mg) was purified by CC over Sephadex LH-20 (MeOH), HPLC (70%→85%, MeOH-H<sub>2</sub>O), and crystallization (MeOH) to afford compounds **15** (5 mg), **18** (3 mg), **20** (22 mg, *t<sub>R</sub>* 27.5 min), and **21** (5 mg, *t<sub>R</sub>* 28.7 min). Fr.3-9 was separated by Sephadex LH-20 (MeOH) and HPLC (10%→40%, MeOH-H<sub>2</sub>O) to yield **26** (3 mg, *t<sub>R</sub>* 33 min). Fr.3-10 was separated by Sephadex LH-20 (MeOH) and HPLC (52%→70%, MeOH-H<sub>2</sub>O) to yield **3** (2 mg, *t<sub>R</sub>* 34 min), **4** (4 mg, *t<sub>R</sub>* 31.5 min), **19** (11 mg), and **27** (3 mg). Fr.3-11 was separated by Sephadex LH-20 (MeOH) and HPLC (55%→70%, MeOH-H<sub>2</sub>O) to yield **1** (8 mg, *t<sub>R</sub>* 33.2 min), **2** (7 mg, *t<sub>R</sub>* 31.5 min), and **25** (4 mg). Fraction Fr.4 (0.9 g) was subjected to CC over ODS with MeOH-H<sub>2</sub>O (20%→100%) and CC on Sephadex LH-20 (MeOH) to yield **28** (3 mg). Fraction Fr.5 (1.2 g) was separated by CC over Sephadex LH-20 (MeOH) and HPLC (5%→20%, MeOH-H<sub>2</sub>O) to yield **8** (70 mg) and **13** (2 mg, *t<sub>R</sub>* 25 min).

*Citreoviridin J* (**1**): Yellow powder;  $[\alpha]_D^{20} - 10$  (c 0.10, MeOH); ECD (MeOH)  $\lambda_{\max}$  ( $\Delta\epsilon$ ) 372 (1.87), 271 (9.81), 216 (6.99) nm; UV (MeOH)  $\lambda_{\max}$  (log  $\epsilon$ ) 196 (3.52), 273 (4.30), 369 (4.31) nm; <sup>1</sup>H and <sup>13</sup>C NMR data, Tables 1 and 2; HRESIMS *m/z* 419.2049 [M + H]<sup>+</sup> (calcd for C<sub>23</sub>H<sub>31</sub>O<sub>7</sub>, 419.2064).

*Citreoviridin K* (**2**): Yellow powder;  $[\alpha]_D^{20} + 2$  (c 0.10, MeOH); ECD (MeOH)  $\lambda_{\max}$  ( $\Delta\epsilon$ ) 373 (1.13), 271 (2.88), 217 (2.54) nm; UV (MeOH)  $\lambda_{\max}$  (log  $\epsilon$ ) 196 (4.50), 274 (4.32), 369 (4.30) nm; <sup>1</sup>H and <sup>13</sup>C NMR data, Tables 1 and 2; HRESIMS *m/z* 419.2063 [M + H]<sup>+</sup> (calcd for C<sub>23</sub>H<sub>31</sub>O<sub>7</sub>, 419.2064).

*Citreoviridin L* (**3**): Yellow powder;  $[\alpha]_D^{20} - 113$  (c 0.10, MeOH); ECD (MeOH)  $\lambda_{\max}$  ( $\Delta\epsilon$ ) 362(3.40), 270 (9.35), 205 (6.88) nm; UV (MeOH)  $\lambda_{\max}$  (log  $\epsilon$ ) 197 (3.68), 273 (4.40), 367 (4.41) nm; <sup>1</sup>H and <sup>13</sup>C NMR data, Tables 1 and 2; HRESIMS *m/z* 419.2056 [M + H]<sup>+</sup> (calcd for C<sub>23</sub>H<sub>31</sub>O<sub>7</sub>, 419.2064).

*Citreoviridin M* (**4**): Yellow powder;  $[\alpha]_D^{20} + 20$  (c 0.10, MeOH); ECD (MeOH)  $\lambda_{\max}$  ( $\Delta\epsilon$ ) 370 (0.70), 272 (8.06), 216 (5.83) nm; UV (MeOH)  $\lambda_{\max}$  (log  $\epsilon$ ) 197 (3.67), 273 (4.45), 369 (4.43) nm; <sup>1</sup>H and <sup>13</sup>C NMR data, Tables 1 and 2; HRESIMS *m/z* 419.2055 [M + H]<sup>+</sup> (calcd for C<sub>23</sub>H<sub>31</sub>O<sub>7</sub>, 419.2064).

*Citreoviridin N* (**5**): Yellow powder;  $[\alpha]_D^{20} - 52$  (c 0.10, MeOH); ECD (MeOH)  $\lambda_{\max}$  ( $\Delta\epsilon$ ) 373 (0.58), 272 (−2.55), 231 (1.27) nm; UV (MeOH)  $\lambda_{\max}$  (log  $\epsilon$ ) 198 (3.67), 272 (4.41), 369 (4.33) nm; <sup>1</sup>H and <sup>13</sup>C NMR data, Tables 1 and 2; HRESIMS *m/z* 419.2045 [M + H]<sup>+</sup> (calcd for C<sub>23</sub>H<sub>31</sub>O<sub>7</sub>, 419.2064).

*Citreoviridin O* (**6**): Yellow powder;  $[\alpha]_D^{20} - 12$  (c 0.10, MeOH); ECD (MeOH)  $\lambda_{\max}$  ( $\Delta\epsilon$ ) 367 (−1.11), 274 (5.18), 211 (−4.03) nm; UV (MeOH)  $\lambda_{\max}$  (log  $\epsilon$ ) 197 (3.43), 274 (4.28), 368 (4.39) nm; <sup>1</sup>H and <sup>13</sup>C NMR data, Tables 1 and 2; HRESIMS *m/z* 419.2042 [M + H]<sup>+</sup> (calcd for C<sub>23</sub>H<sub>31</sub>O<sub>7</sub>, 419.2064).



### 3.5. ECD Calculation

The conformational analysis was first performed via random searching in the Stochastic using the MMFF94 force field with an energy cutoff of 7.0 kcal/mol and an RMSD threshold of 0.2 Å. All conformers were consecutively optimized at the PM6 and HF/6-31G(d) levels. Dominative conformers were re-optimized at the B3LYP/6-31G(d) level in the gas phase. The theoretical ECD spectra were calculated with the B3LYP method at the 6-311G(d,p) level in MeOH using Gaussian 09. The ECD spectrum was simulated by overlapping Gaussian functions for each transition [41].

### 3.6. Measurement of ICD Spectra

Compounds 1–6 were first dissolved in appropriate DMSO. Then, a quantity of  $\text{Mo}_2(\text{OAc})_4$  were added, with a ligand-to-metal ratio of approximately 1:1.2. The first CD spectrum ( $\text{CD}_0$ ) was recorded immediately after mixing and scanned every 10 min until a stationary CD spectrum ( $\text{CD}_1$ ) was measured. The induced CD (ICD) spectra were calculated from the CD of the ligand–metal complex ( $\text{CD}_1$ ) deducting the inherent CD ( $\text{CD}_0$ ).

### 3.7. The Antiproliferative Bioassay

As reported previously, the experiment was conducted using the Cell Counting Kit-8 (CCK-8) assay [42]. Briefly, HeLa cells were seeded in a 96-well plate at a density of 2000 cells/well and were cultured in MEM/EBSS (MEM) containing 10% FBS at 37 °C. After 24 h, the cells were treated with the test compounds, and incubation continued for 72 h. Then, 10 µL CCK-8 solution was added to each well. After incubation at 37 °C for 4 h, the absorbance value of each well was determined using a multi-well plate reader at 450 nm.

### 3.8. Flow Cytometry

After the indicated time treatment, cancer cell arrest was assessed by an FACScan flow cytometer (Beckman Coulter, California, USA), following the manual procedure. The cells were harvested by trypsin digestion, washed with PBS, and fixed with ice-cold 70% ethanol at 4 °C overnight. The fixed cells were then washed twice in PBS and treated for 30 min at RT with propidium iodide in PBS and analyzed. Flow cytometry data were analyzed using CytExpert (Beckman Coulter).

### 3.9. Western Blot Analysis

For Western blot assays, HeLa cells were treated with the compounds for the indicated time. Then, the cells were harvested, lysed, and centrifuged at 12,000 rpm/min for 10 min. The supernatant was added with a 1/5 volume of 5 × SDS and boiled. After electrophoresis, protein samples were transferred to the PVDF film, blocked with fat-free milk, incubated with the first antibody and washed, and then incubated with the secondary antibody and washed. Then, the ECL droplets were reacted on the membrane surface, and the bands were imaged by the multifunctional chemiluminescence imaging system.

## 4. Conclusions

From the deep-sea-derived *Penicillium citreonigrum* MCCC 3A00169, 6 new and 22 known compounds were obtained. Compounds 7, 14, and 20 significantly induced apoptosis against HeLa cells with  $\text{IC}_{50}$  values of 5.4 µM, 11.3 µM, and 0.7 µM.

**Supplementary Materials:** The following supporting information can be downloaded at: <https://www.mdpi.com/article/10.3390/md20120736/s1>, Figure S1: Chemical structures of compounds 7–28; Figures S2–S54: The 1D-NMR, 2D-NMR, and HRMS spectra of compounds 1–6.

**Author Contributions:** J.-S.W., X.-W.Y. and X.-K.Z. designed and coordinated the project. Z.-B.Z., C.-L.X. and M.-M.X. isolated and purified all compounds. Y.-Q.Z. conducted the bioactive experiments. L.X. and Y.-J.H. performed the fermentation. Z.-B.Z., G.Z., L.-Z.L. and X.-W.Y. analyzed the

data and wrote the paper, while critical revision of the publication was performed by all authors. All authors have read and agreed to the published version of the manuscript.

**Funding:** The work was supported by the National Natural Science Foundation of China (22177143 and 21877022) and the Science and Technology Research Program of Xiamen Medical College (KPT2020-03).

**Institutional Review Board Statement:** Not applicable.

**Informed Consent Statement:** Not applicable.

**Conflicts of Interest:** The authors declare no conflict of interest.

## References

1. Uchiyama, Y.; Takino, M.; Noguchi, M.; Shiratori, N.; Kobayashi, N.; Sugita-Konishi, Y. The In vivo and in vitro toxicokinetics of citreoviridin extracted from *Penicillium citreonigrum*. *Toxins* **2019**, *11*, 360. [[CrossRef](#)] [[PubMed](#)]
2. Wang, X.; Sena Filho, J.G.; Hoover, A.R.; King, J.B.; Ellis, T.K.; Powell, D.R.; Cichewicz, R.H. Chemical epigenetics alters the secondary metabolite composition of guttate excreted by an atlantic-forest-soil-derived *Penicillium citreonigrum*. *J. Nat. Prod.* **2010**, *73*, 942–948. [[CrossRef](#)] [[PubMed](#)]
3. Yuan, W.H.; Wei, Z.W.; Dai, P.; Wu, H.; Zhao, Y.X.; Zhang, M.M.; Jiang, N.; Zheng, W.F. Halogenated metabolites isolated from *Penicillium citreonigrum*. *Chem. Biodivers.* **2014**, *11*, 1078–1087. [[CrossRef](#)] [[PubMed](#)]
4. Huang, J.N.; Zou, Q.B.; Chen, J.; Xu, S.H.; Luo, D.; Zhang, F.G.; Lu, Y.Y. Phenols and diketopiperazines isolated from antarctic-derived fungi, *Penicillium citreonigrum* SP-6. *Phytochem. Lett.* **2018**, *27*, 114–118. [[CrossRef](#)]
5. Tang, X.X.; Liu, S.Z.; Yan, X.; Tang, B.W.; Fang, M.J.; Wang, X.M.; Wu, Z.; Qiu, Y.K. Two new cytotoxic compounds from a deep-sea *Penicillium citreonigrum* XT20-134. *Mar. Drugs* **2019**, *17*, 509. [[CrossRef](#)]
6. Yuan, W.H.; Goto, M.; Hsieh, K.Y.; Yuan, B.; Zhao, Y.; Morris-Natschke, S.L.; Lee, K.H. Selective cytotoxic eremophilane-type sesquiterpenes from *Penicillium citreonigrum*. *J. Asian Nat. Prod. Res.* **2015**, *17*, 1239–1244. [[CrossRef](#)]
7. Yuan, W.H.; Zhang, Y.; Zhang, P.; Ding, R.R. Antioxidant sesquiterpenes from *Penicillium citreonigrum*. *Nat. Prod. Commun.* **2017**, *12*, 1827–1829. [[CrossRef](#)]
8. Sun, C.X.; Mudassir, S.; Zhang, Z.Z.; Feng, Y.Y.; Chang, Y.M.; Che, Q.; Gu, Q.Q.; Zhu, T.J.; Zhang, G.J.; Li, D.H. Secondary metabolites from deep-sea derived microorganisms. *Curr. Med. Chem.* **2020**, *27*, 6244–6273. [[CrossRef](#)]
9. Xie, C.L.; Zhang, D.; Guo, K.Q.; Yan, Q.X.; Zou, Z.B.; He, Z.H.; Wu, Z.; Zhang, X.K.; Chen, H.F.; Yang, X.W. Meroterpenothiazole A, a unique meroterpenoid from the deep-sea-derived *Penicillium allii-sativi*, significantly inhibited retinoid X receptor (RXR)- $\alpha$  transcriptional effect. *Chin. Chem. Lett.* **2022**, *33*, 2057–2059. [[CrossRef](#)]
10. Niu, S.; Xie, C.L.; Xia, J.M.; Liu, Q.M.; Peng, G.; Liu, G.M.; Yang, X.W. Botryotins A–H, tetracyclic diterpenoids representing three carbon skeletons from a deep-sea-derived *Botryotinia fuckeliana*. *Org. Lett.* **2020**, *22*, 580–583. [[CrossRef](#)]
11. Niu, S.; Xia, J.M.; Li, Z.; Yang, L.H.; Yi, Z.W.; Xie, C.L.; Peng, G.; Luo, Z.H.; Shao, Z.; Yang, X.W. Aphidicolin chemistry of the deep-sea-derived fungus *Botryotinia fuckeliana* MCCC 3A00494. *J. Nat. Prod.* **2019**, *82*, 2307–2331. [[CrossRef](#)] [[PubMed](#)]
12. Zhang, H.; Mao, L.L.; Qian, P.T.; Shan, W.G.; Wang, J.D.; Bai, H. Two new metabolites from a soil fungus *Curvularia affinis* strain HS-FG-196. *J. Asian Nat. Prod. Res.* **2012**, *14*, 1078–1083. [[CrossRef](#)] [[PubMed](#)]
13. Koga, J.; Yamauchi, T.; Shimura, M.; Ogawa, N.; Oshima, K.; Umemura, K.; Kikuchi, M.; Ogasawara, N. Cerebrosides A and C, sphingolipid elicitors of hypersensitive cell death and phytoalexin accumulation in rice plants. *J. Biol. Chem.* **1998**, *273*, 31985–31991. [[CrossRef](#)]
14. Guo, R.H.; Zhang, Y.T.; Duan, D.; Fu, Q.; Zhang, X.Y.; Yu, X.W.; Wang, S.J.; Bao, B.; Wu, W.H. Fibrinolytic evaluation of compounds isolated from a marine fungus *Stachybotrys longispora* FG216. *Chin. J. Chem.* **2016**, *34*, 1194–1198. [[CrossRef](#)]
15. Zhao, D.; Zheng, L.; Qi, L.; Wang, S.; Guan, L.; Xia, Y.; Cai, J. Structural features and potent antidepressant effects of total sterols and beta-sitosterol extracted from *Sargassum horneri*. *Mar. Drugs* **2016**, *14*, 123. [[CrossRef](#)] [[PubMed](#)]
16. Uegaki, R.; Fujimori, T.; Kaneko, H.; Kato, K.; Noguchi, M. Isolation of dehydrololiolide and 3-oxo-actinidol from *Nicotiana tabacum*. *Agric. Biol. Chem.* **1979**, *43*, 1149–1150. [[CrossRef](#)]
17. Tanimoto, S.; Tominaga, H.; Okada, Y.; Nomura, M. Synthesis and cosmetic whitening effect of glycosides derived from several phenylpropanoids. *Yakugaku. Zasshi.* **2006**, *126*, 173–177. [[CrossRef](#)]
18. Arakawa, M.; Someno, T.; Kawada, M.; Ikeda, D. A new terrein glucoside, a novel inhibitor of angiogenin secretion in tumor angiogenesis. *J. Antibiot.* **2008**, *61*, 442–448. [[CrossRef](#)]
19. Wang, C.Y.; Wang, B.G.; Brauers, G.; Guan, H.S.; Proksch, P.; Ebel, R. Microsphaerones A and B, two novel gamma-pyrone derivatives from the sponge-derived fungus *Microsphaeropsis* sp. *J. Nat. Prod.* **2002**, *65*, 772–775. [[CrossRef](#)]
20. You, J.; Yang, S.Z.; Mu, B.Z. Structural characterization of lipopeptides from *Enterobacter* sp strain N18 reveals production of surfactin homologues. *Eur. J. Lipid Sci. Technol.* **2015**, *117*, 890–898. [[CrossRef](#)]
21. Nagia, M.M.; El-Metwally, M.M.; Shaaban, M.; El-Zalabani, S.M.; Hanna, A.G. Four butyrolactones and diverse bioactive secondary metabolites from terrestrial *Aspergillus flavipes* MM2: Isolation and structure determination. *Org. Med. Chem. Lett.* **2012**, *2*, 9. [[CrossRef](#)] [[PubMed](#)]

22. Zhang, Y.Y.; Zhang, Y.; Yao, Y.B.; Lei, X.L.; Qian, Z.J. Butyrolactone-I from coral-derived fungus *Aspergillus terreus* attenuates neuro-inflammatory response via suppression of NF-kappaB Pathway in BV-2 Cells. *Mar. Drugs* **2018**, *16*, 202. [[CrossRef](#)] [[PubMed](#)]
23. da Rocha, M.W.; Resck, I.S.; Caldas, E.D. Purification and full characterisation of citreoviridin produced by *Penicillium citreonigrum* in yeast extract sucrose (YES) medium. *Food Addit. Contam. Part A* **2015**, *32*, 584–595. [[CrossRef](#)] [[PubMed](#)]
24. Xu, K.; Li, G.; Zhu, R.; Xie, F.; Li, Y.; Yang, W.; Xu, L.; Shen, T.; Zhao, Z.; Lou, H. Polyketides from the endolichenic fungus *Eupenicillium javanicum* and their anti-inflammatory activities. *Phytochemistry* **2020**, *170*, 112191. [[CrossRef](#)]
25. Li, J.; Wang, J.; Jiang, C.S.; Li, G.; Guo, Y.W. (+)-Cyclophenol, a new naturally occurring 7-membered 2,5-dioxopiperazine alkaloid from the fungus *Penicillium sclerotiorum* endogenous with the Chinese mangrove *Bruguiera gymnorrhiza*. *J. Asian Nat. Prod. Res.* **2014**, *16*, 542–548. [[CrossRef](#)]
26. Campos, P.E.; Pichon, E.; Moriou, C.; Clerc, P.; Trepos, R.; Frederich, M.; De Voogd, N.; Hellio, C.; Gauvin-Bialecki, A.; Al-Mourabit, A. New antimalarial and antimicrobial tryptamine derivatives from the marine sponge *Fascaplysinopsis reticulata*. *Mar. Drugs* **2019**, *17*, 167. [[CrossRef](#)]
27. Wang, X.Y.; Liu, Y.Z.; Xu, J.; Jiang, F.W.; Kang, C.M. Synthesis of novel indole-benzimidazole derivatives. *J. Chem. Res.* **2016**, *40*, 588–590. [[CrossRef](#)]
28. Hashida, J.; Niitsuma, M.; Iwatsuki, M.; Mori, M.; Ishiyama, A.; Namatame, M.; Nishihara-Tsukashima, A.; Nonaka, K.; Ui, H.; Masuma, R.; et al. Pyrenocine I, a new pyrenocine analog produced by *Paecilomyces* sp. FKI-3573. *J. Antibiot.* **2010**, *63*, 559–561. [[CrossRef](#)]
29. Nakada, T.; Sudo, S.; Kosemura, S.; Yamamura, S. Two new metabolites of hybrid strains KO 0201 and 0211 derived from *Penicillium citreoviride* B. IFO 6200 and 4692. *Tetrahedron Lett.* **1999**, *40*, 6831–6834. [[CrossRef](#)]
30. Hallock, Y.F.; Clardy, J.; Kenfield, D.S.; Strobel, G. De-O-methyladiaporthin, a phytotoxin from *Drechslera siccas*. *Phytochemistry* **1988**, *27*, 3123–3125. [[CrossRef](#)]
31. Yamaguchi, Y.; Masuma, R.; Kim, Y.-P.; Uchida, R.; Tomoda, H.; Omura, S. Taxonomy and secondary metabolites of *Pseudobotrytis* sp. FKA-25. *Mycoscience* **2004**, *45*, 9–16. [[CrossRef](#)]
32. Chen, C.; Ye, G.; Tang, J.; Li, J.; Liu, W.; Wu, L.; Long, Y. New polyketides from mangrove endophytic fungus *Penicillium* sp. BJR-P2 and their anti-inflammatory activity. *Mar. Drugs* **2022**, *20*, 583. [[CrossRef](#)] [[PubMed](#)]
33. Frelek, J.; Ikekawa, N.; Takatsuto, S.; Snatzke, G. Application of [Mo<sub>2</sub>(OAc)<sub>4</sub>] for determination of absolute configuration of brassinosteroid vic-diols by circular dichroism. *Chirality* **1997**, *9*, 578–582. [[CrossRef](#)]
34. Frelek, J.; Klimek, A.; Ruskowska, P. Dinuclear transition metal complexes as auxiliary chromophores in chiroptical studies on bioactive compounds. *Curr. Org. Chem.* **2003**, *7*, 1081–1104. [[CrossRef](#)]
35. Frelek, J.; Pakulski, Z.; Zamojski, A. Application of [Mo<sub>2</sub>(OAc)<sub>4</sub>] for determination of absolute configuration of pyranoid and furanoid vic-diols by circular dichroism. *Tetrahedron Asymmetry* **1996**, *7*, 1363–1372. [[CrossRef](#)]
36. Górecki, M.; Jabłońska, E.; Kruszewska, A.; Suszczyńska, A.; Urbańczyk-Lipkowska, Z.; Gerards, M.; Morzycki, J.W.; Szczeppek, W.J.; Frelek, J. Practical method for the absolute configuration assignment of tert/tert 1,2-diols using their complexes with Mo<sub>2</sub>(OAc)<sub>4</sub>. *J. Org. Chem.* **2007**, *72*, 2906–2916. [[CrossRef](#)]
37. Hou, H.; Zhou, R.; Li, A.; Li, C.; Li, Q.; Liu, J.; Jiang, B. Citreoviridin inhibits cell proliferation and enhances apoptosis of human umbilical vein endothelial cells. *Environ. Toxicol. Pharmacol.* **2014**, *37*, 828–836. [[CrossRef](#)]
38. Myobatake, Y.; Kamisuki, S.; Tsukuda, S.; Higashi, T.; Chinen, T.; Takemoto, K.; Hachisuka, M.; Suzuki, Y.; Takei, M.; Tsurukawa, Y.; et al. Pyrenocine A induces monopolar spindle formation and suppresses proliferation of cancer cells. *Bioorg. Med. Chem.* **2019**, *27*, 115149. [[CrossRef](#)]
39. Buachan, P.; Namsa-Aid, M.; Sung, H.K.; Peng, C.; Sweeney, G.; Tanechpongamb, W. Inhibitory effects of terrein on lung cancer cell metastasis and angiogenesis. *Oncol. Rep.* **2021**, *45*, 94. [[CrossRef](#)]
40. Feng, C.; Li, D.; Chen, M.; Jiang, L.; Liu, X.; Li, Q.; Geng, C.; Sun, X.; Yang, G.; Zhang, L.; et al. Citreoviridin induces myocardial apoptosis through PPAR-gamma-mTORC2-mediated autophagic pathway and the protective effect of thiamine and selenium. *Chem. Biol. Interact.* **2019**, *311*, 108795. [[CrossRef](#)]
41. Zou, Z.B.; Zhang, G.; Li, S.M.; He, Z.H.; Yan, Q.X.; Lin, Y.K.; Xie, C.L.; Xia, J.M.; Luo, Z.H.; Luo, L.Z.; et al. Asperochratides A–J, ten new polyketides from the deep-sea-derived *Aspergillus ochraceus*. *Bioorg. Chem.* **2020**, *105*, 104349. [[CrossRef](#)] [[PubMed](#)]
42. Xiao, H.X.; Yan, Q.X.; He, Z.H.; Zou, Z.B.; Le, Q.Q.; Chen, T.T.; Cai, B.; Yang, X.W.; Luo, S.L. Total synthesis and anti-inflammatory bioactivity of (–)-majusculoic acid and its derivatives. *Mar. Drugs* **2021**, *19*, 288. [[CrossRef](#)] [[PubMed](#)]